Core–shell Zn-doped TiO_2–ZnO nanofibers fabricated *via* a combination of electrospinning and metal–organic chemical vapour deposition

M. E. Fragalà,*[a] I. Cacciotti,[b] Y. Aleeva,[a] R. Lo Nigro,[c] A. Bianco,[b] G. Malandrino,[a] C. Spinella,[c] G. Pezzotti[d] and G. Gusmano[b]

Received 10th March 2010, Accepted 11th May 2010
DOI: 10.1039/c004157b

Zn-doped TiO_2 nanofibers shelled with ZnO hierarchical nanoarchitectures have been fabricated combining electrospinning of TiO_2 (anatase) nanofibers and metal–organic chemical vapor deposition (MOCVD) of ZnO. The proposed hybrid approach has proven suitable for tailoring both the morphology of the ZnO external shell as well as the crystal structure of the Zn-doped TiO_2 core. It has been found that the Zn dopant is incorporated in calcined electrospun nanofibers without any evidence of ZnO aggregates. Effects of different Zn doping levels of Zn-doped TiO_2 fibers have been scrutinized and morphological, structural, physico-chemical and optical properties evaluated before and after the hierarchical growth of the external ZnO shell over the electrospun nanofibers. Moreover, doping promotes the incipient transition from the anatase to rutile phase in the core–shell Zn-doped TiO_2–ZnO nanostructures at lower temperature than that observed for pure TiO_2. Finally, the present core–shell hierarchical nanofibers possess a very large surface to volume ratio and exhibit a marked cathodoluminescence with a strong UV and visible emission.

Introduction

Hierarchical hetero-nanostructures[1] find applications in a variety of fields such as field emission[2] photovoltaics,[3] supercapacitors,[4] fuel cells[5] and multifunctional nanocomposites[6] that require high surface areas. Synthetic routes suited for enhancing robustness and controlling sizes, shapes, and compositions have therefore received increasing attention in recent years. In this scenario, metal oxide semiconductors having dual or multiple morphologies and structures, become of interest since they represent a versatile solution for performance enhancement and applications in multifunctional devices.[7]

In particular, great attention has been recently devoted to the fabrication of nanocomposites containing ZnO and TiO_2.[8–11] In fact, implementation of TiO_2 materials with ZnO has often proved to improve the photocatalytic properties of TiO_2[8,12] and to promote some anatase-to-rutile phase transition.[13] Actually, the co-existence of these two phases due to the presence of dopant heteroatoms[13–15] appears particularly promising since it modifies the spatial charge separation and reduces the recombination efficiency, hence improving the photocatalytic performances.[16]

In addition, ZnO hierarchical nanostructures are excellent sensors (*i.e.* gas,[17–19] humidity, [20] UV[21]) due to the enhanced surface interactions depending on a more favorable surface to volume ratio than ZnO bulk and continuous nanostructured films.

The recent interest toward electrospun TiO_2 nanofibers as a structural alternative to nanoparticle-based electrodes in dye sensitive solar cells (DSSCs)[22] is another motivation to study ZnO–TiO_2 composite nanofiber materials.[23] Finally, electrospun nanofibers have been recently used as nanoplatforms for gas sensors[23,24] and several approaches have been adopted for functional activation of their surfaces.[25,26]

Therefore, any effort to enhance the working surface area of the multifunctional devices can successfully take advantages of three-dimensional (3-D) nanostructured materials and hierarchical single-crystal branches of smaller size represent an effective approach for surface activation.[27]

In this context, we report here on the successful fabrication and full characterization of Zn-doped TiO_2 electrospun nanofibers (herein d:TiO_2) shelled *via* MOCVD deposition with hierarchical ZnO nanostructures. The present approach combines the flexibility of electrospinning to large-scale production of ceramic nanofibers[28] with all the MOCVD benefits associated with high reproducibility, easily controlled growth (largely proven on large scale), short process times, quality grade crystallinity and elemental purity. Presently, this strategy has been successfully tested for the reproducible fabrication of standing alone d:TiO_2 as well as of core nanofibers shelled with ZnO hierarchical nanostructures (herein d:TiO_2–ZnO). The particularly favorable surface-to-volume ratio, due in turn to the large density of ZnO single crystalline nanorods/nanoneedles on the shell surface, promotes a remarkable cathodoluminescence emission in the UV and visible regions. The obtained nanoarchitectures are quite complex and therefore a careful characterization of the Zn-doped TiO_2 core, before and after the ZnO external shell deposition, is herein presented.

[a]*Dipartimento di Scienze Chimiche Università di Catania and INSTM UdR Catania, Viale Andrea Doria, 6, 95125 Catania, Italy. E-mail: me.fragala@unict.it*
[b]*University of Rome "Tor Vergata", Dipartimento di Scienze e Tecnologie Chimiche, INSTM UdR, Roma Tor Vergata, Via della Ricerca Scientifica, 00133 Rome, Italy*
[c]*Istituto per la Microelettronica e Microsistemi, IMM CNR, Strada VII Zona industriale n 5, 95121 Catania, Italy*
[d]*Ceramic Physics Laboratory & Research Institute for Nanoscience, Kyoto Institute of Technology, Matsugasaki, Sakyo-ku, Kyoto, 606-8585, Japan*

Results and discussions

Fabrication and characterization of TiO_2 and Zn-doped TiO_2 (d:TiO_2) electrospun nanofiber templates

Uniform one-dimensional (1-D) hybrid nanofibers have been fabricated by electrospinning from alcoholic solutions of polyvinylpyrrolidone (PVP) and suitable alcoholic precursors of titanium(IV) and zinc(II) ions, namely titanium tetraisopropoxide and $Zn(tta)_2tmeda$[29] (Htta = 2-thenoyl-trifluoroacetone, tmeda = *N*,*N*,*N*′,*N*′-tetramethylethylendiamine). The relative atomic concentration of the Zn metal–organic precursor has been varied from 3% to 15%.

Electrospun Zn-doped TiO_2/PVP nanofibers have been calcined in air at 500 °C for 3 h to completely remove the polymeric component as well as to promote the complete decomposition of Zn(II) metal–organic precursor inside the nanofibers. All electrospun materials, after thermal treatment at 500 °C, consist of randomly oriented fibers with average diameters of 50 ± 30 nm. Large interconnected voids are present among the fibers, thus resulting in a 3D porous network.

Fig. 1 shows an SEM image of d:TiO_2 nanofibers, deposited on Si substrate and calcined at 500 °C. The related EDX analyses point to the presence of Zn heteroatoms with a TiO_2/Zn composition in the nanofibers well in agreement with nominal values (Table 1). The bright field transmission electron microscopy (TEM) image (Fig. 2a) confirms the presence of polycrystalline nanofibers having different size ranging from 20 to 100 nm. The energy-filtered TEM (EF-TEM) maps provide evidence of a homogeneous chemical distribution of both Ti and Zn ions (Fig. 2b and 2c) in agreement with the presence of well distributed Zn dopant without aggregation of ZnO grains. These findings match well with XRD data of d:TiO_2 nanofibers (Fig. 3). In fact, the obtained patterns show the sequence of broad peaks expected for the pure anatase TiO_2 phase (JCPDS #21-1272) without any evidence of spectral

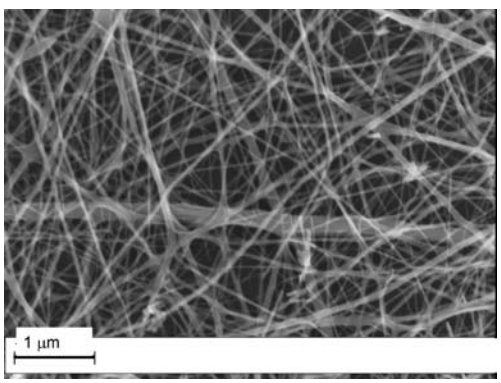

Fig. 1 SEM image of the d:TiO_2 (Zn 15%) electrospun nanofibers.

Table 1 EDX analyses of the d:TiO_2 nanofibers

Nominal Zn/Ti%	Zn/Ti at%
3%	3.1
5%	5.4
15%	14.8

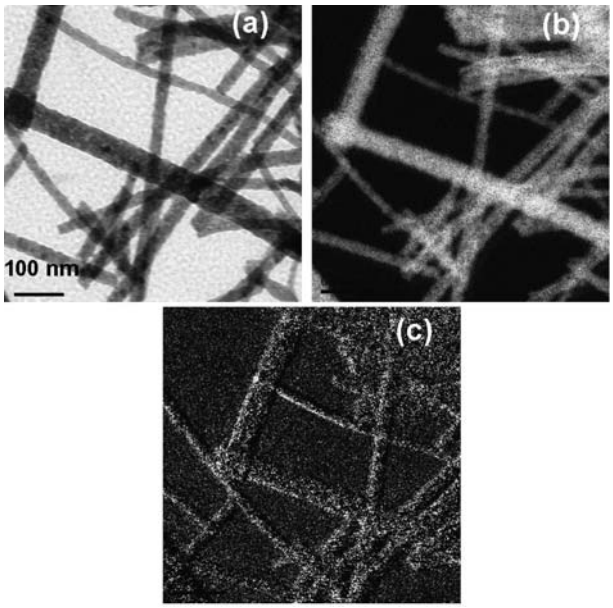

Fig. 2 Bright field TEM image of the d:TiO_2 (Zn 15%) nanofibers (a); Energy Filtered TEM maps of Ti (b) and Zn (c). Bar is 100 nm.

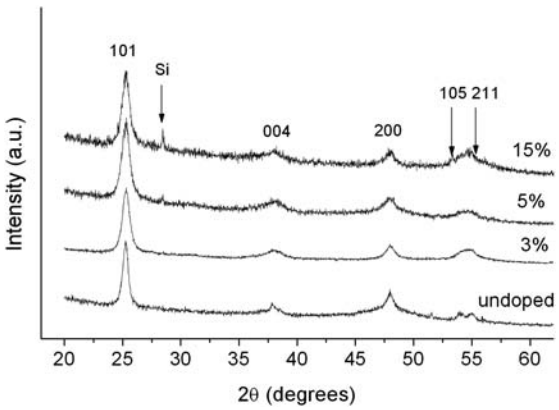

Fig. 3 XRD patterns of calcined (500 °C, 3 h) undoped TiO_2 and Zn doped TiO_2 electrospun nanofibers.

features that might be related to ZnO. This points to the lack of any crystalline ZnO precipitate inside the TiO_2 nanofibers, even after calcination at 500 °C in air.

The XPS survey spectra (Fig. 4a) of calcined d:TiO_2 nanofibers show, in addition to Ti, O and C features observed in the undoped reference, the Zn core level peaks. The undoped nanofibers present the Ti 2p doublet (Fig. 4b) in the 458.9–464.6 eV range, with the spin orbit splitting (5.7 eV) in good agreement with the Ti^{4+} oxidation state.[29] Upon increasing the Zn content in the nanofibers, this feature slightly moves towards lower binding energy.[30] Even more significant modifications are observed in the case of the O1s peak (Fig. 4c). The undoped TiO_2 reference shows an asymmetrical and well discernible broadening toward higher binding energy values that highlights two rather resolved components centred at 530.3 eV and at 532.2 eV, respectively. Literature data[31,32] suggest that the low energy component represents the Ti–O bonds while the high energy tail can be

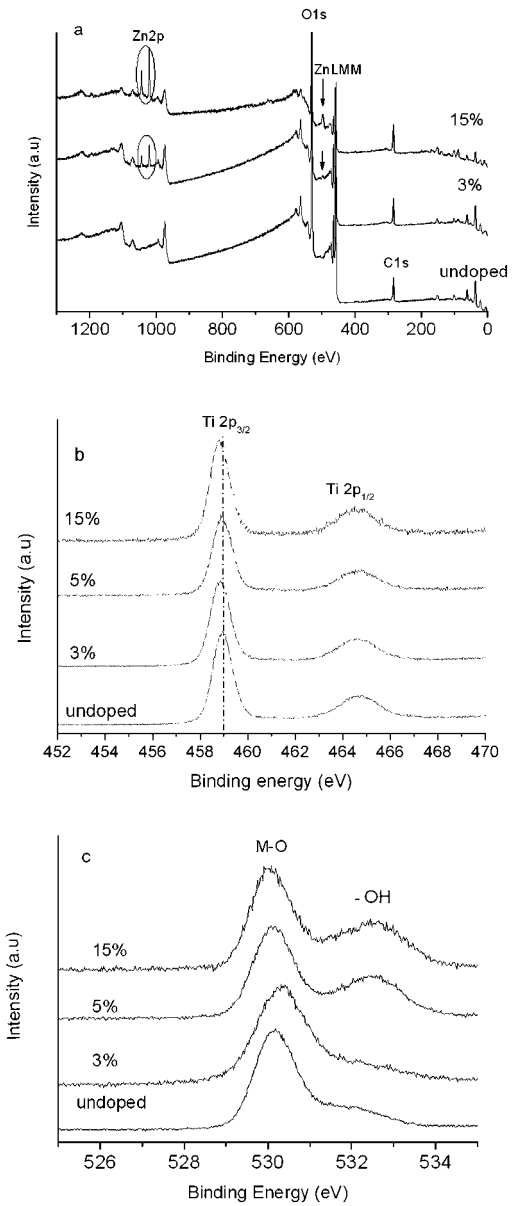

Fig. 4 XPS survey of calcined undoped TiO_2 and Zn doped TiO_2 electrospun nanofibers (a); high resolution XPS spectra of Ti 2p (b) and O1s (c) regions of calcined undoped TiO_2 and Zn doped TiO_2 nanofibers.

related to hydroxyl groups (OH^-) over the nanofiber surface. Upon increasing the Zn content in the nanofibers the relative intensity of the latter feature increases, thus pointing to a higher surface hydroxylation.[12]

Finally, the Zn2p region (see the detail indicated in Fig. 4a) shows the expected $Zn2p_{3/2,1/2}$ doublet at 1022.0 eV and 1045.0 eV, respectively. The inferred spin orbit splitting (23 eV) is indicative of a Zn^{2+} ion. Chemical shifts associated with Zn-containing compounds are normally spread in a narrow range and, therefore, poorly suited for identification of the oxidation state. Nevertheless, the Auger parameter (α) is indicative of chemical state. In the present case, the measured Auger parameter ($\alpha = 2010$ eV)[33] can be associated with Zn^{2+} on the surface of TiO_2-based nanofibers. It, therefore, transpires that calcination at 500 °C causes an exhaustive

Table 2 XPS atomic compositional data of d:TiO_2 nanofibers and Zn Auger parameters

Nominal Zn %	Zn %	Ti %	O %	C %[a]	Zn α parameter (eV)
3	2	20	58	20	2010.1
5	3	20	57	20	2010.3
15	8	16	55	21	2010.2

[a] The XPS spectra were recorded without any sputtering process, thus the C content arises from surface carbon contamination.

decomposition of the Zn precursor. Table 2 collects the Auger parameters and atomic compositional data of calcined d:TiO_2 nanofibers. Analytical data have been evaluated from XPS peak areas, corrected for their relative sensitivity factors. It becomes evident that the Zn-doping levels obtained from XPS are much higher than the nominal values (the latter confirmed by the EDX data, as shown in Table 1). Note that XPS results refer to the surface composition and provide an indication of Zn surface segregation on the TiO_2 nanofibers, while the EDX data relate to the bulk composition. The C content is mainly related to surface contamination that is particularly significant due to the large surface to volume ratio of the present system. In order to avoid any kind of fiber damage, no sputtering has been performed before XPS analysis. For the sake of completeness, the C content associated with incomplete precursor decomposition of as spun nanofibers (not shown) is about 60%.

The present d:TiO2 nanofibers have been used as a template (thus providing flexibility, self-standing properties and high surface-to-volume ratio) to produce core–shell hierarchical d:TiO_2–ZnO nanoarchitectures *via* MOCVD.

In this perspective, undoped and d:TiO_2 (Zn 5%) nanofibers have been annealed at 600 °C under a reduced pressure O_2/Ar atmosphere. XRD studies have given insight into the role played by the dopant on the anatase-to-rutile transition. In Fig. 5, the XRD diffraction pattern of undoped TiO_2 nanofibers is compared with that of the d:TiO_2 (Zn 5%) sample. The presence of the rutile most predominant peak at $2\theta = 27.48°$ (JCPDS #73-1765) in the d:TiO_2 pattern indicates that Zn doping induces the anatase to rutile transition at 600 °C.

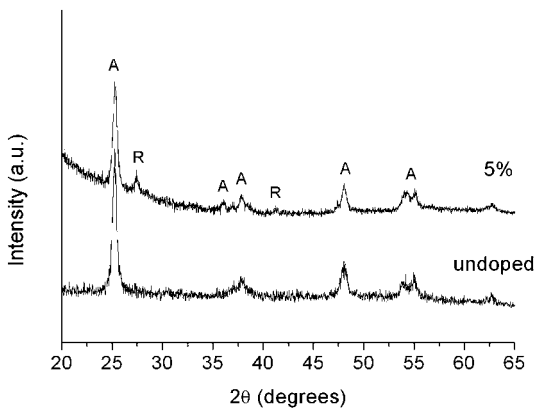

Fig. 5 XRD patterns of annealed (600 °C, 1 h, O_2/Ar) TiO_2 and Zn-doped TiO_2 nanofibers.

Fabrication and characterization of core–shell TiO_2–ZnO and d:TiO_2–ZnO electrospun nanofibers

The calcined electrospun d:TiO_2 nanofibers represent suitable nanoplatforms for fabrication of hierarchical ZnO nanostructures *via* MOCVD. The ZnO shell nanostructures have been deposited at 600 °C for 60 min on undoped and d:TiO_2 nanofibers. SEM micrographs (Fig. 6a–d) provide evidence of surface hierarchical ZnO nanostructures. Decoration on the nanofibers generally consists of nanograins or shorter nanorods. The XRD patterns (Fig. 7) of the d:TiO_2–ZnO core–shell nanofibers provide evidence of formation of polycrystalline ZnO (JCPDS # 36-1451) and of the anatase-to-rutile transition promoted by ZnO doping.[12,34] In addition, interaction of ZnO shell and TiO_2 core gives rise to a sizeable formation of a mixed ZnO–TiO_2 phase (Ecandrewsite JCPDS # 26-1500) and of Zn_2TiO_4 (JCPDS # 25-1164).

Longer deposition times (90 *vs.* 60 min) cause the growth of thin and longer nanoneedles (Fig. 8). Both nature and architecture of such nanofibers have been proved by TEM investigation (Fig. 9). Contrast evaluation indicates that core nanofibers are certainly polycrystalline in accordance with XRD data with a mean 20–30 nm grain size. Hierarchical ZnO nanoneedles are, by contrast, monocrystalline with tip dimension ranging from 8 to 20 nm. The energy-filtered chemical oxygen map shows a homogeneous intensity distribution. By contrast, the Ti and Zn maps provide clear evidence that Ti is present only on the main body while Zn is distributed on the main nanofiber and the external nanoneedles. It must be noted that the Zn signal associated with the central nanofiber can be due to both the MOCVD ZnO decoration as well as to the Zn doping of the TiO_2 nanofibers. Further insights into the MOCVD deposited ZnO nanoneedles have been obtained by high resolution TEM imaging (Fig. 10). The HR-TEM image points to the formation of ZnO single-crystal nanoneedles, while the reduced Fast Fourier Transform (FFT) image (inset of Fig. 10) shows that the lattice spacing (5.16 Å) along the *c*-axis indicates the [0001] as the direction growth of ZnO nanoneedles.

Optical properties of the present nanostructures have been also studied by cathodoluminescence. Spectra of the TiO_2 and d:TiO_2 nanofibers, before and after ZnO MOCVD decoration, are reproduced in Fig. 11. Before ZnO shell deposition, the spectra of the TiO_2 and of d:TiO_2 nanofibers were characterised by the green broad emission band, centered around 550 nm, that relates to surface defects of TiO_2.[35] This band shifts to 500 nm in the core–shell d:TiO_2–ZnO nanofibers mainly due to ZnO surface intrinsic defects.[36,37] Different mechanisms have been proposed to explain the origin of the ZnO green emission band. In particular, a strong correlation between the green emission, the free-carriers concentration and the density of singly ionized vacancies in commercial ZnO phosphor powders has often been highlighted.[38–41] The green emission in ZnO phosphors is thus a result of the recombination of one electron in singly occupied oxygen vacancies with photoexcited holes in the valence band.[42] Moreover, the cathodoluminescence experiments on core–shell d:TiO_2–ZnO provide evidence of a relatively sharp ultraviolet (UV) emission peak centred at 383 nm, corresponding to the near band edge (NBE) emission of the ZnO crystal. This band can be attributed to the recombination of free excitons.[43] It is known

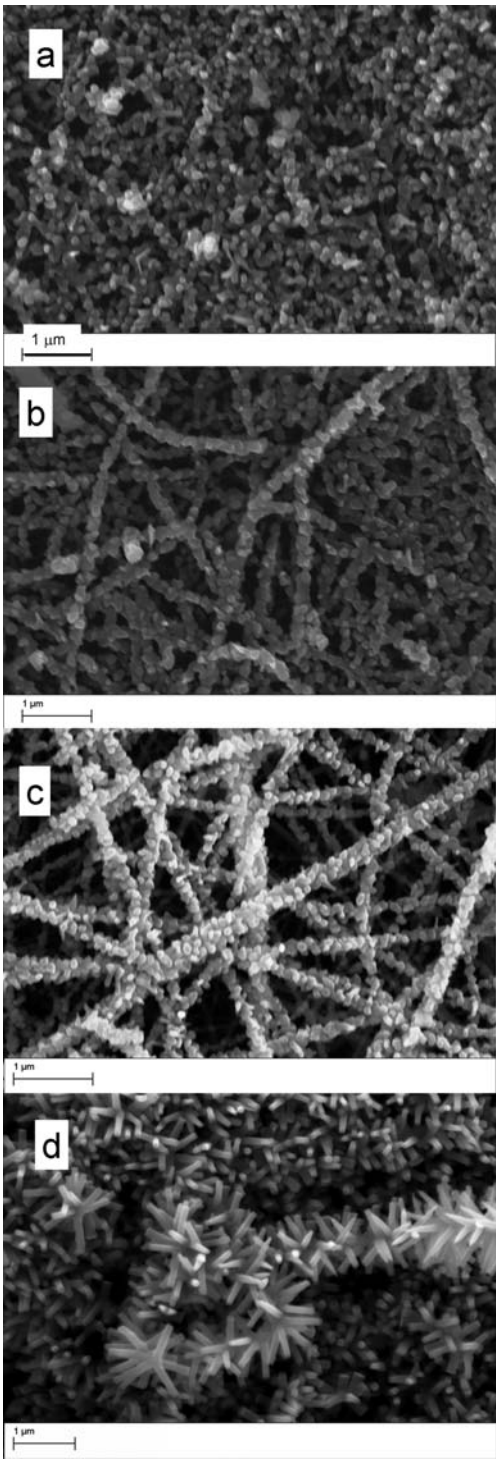

Fig. 6 SEM images of core–shell TiO_2–ZnO nanofibers (a); d:TiO_2–ZnO nanofibers (Zn 3%) (b); d:TiO_2–ZnO (Zn 5%) nanofibers (c); d:TiO_2–ZnO nanofibers (Zn 15%) (d). The decorating ZnO shell is deposited by MOCVD at 600 °C for 60 min.

that the band edge emission of semiconductors strongly depends on the quality of the crystal. In the present case, this ultraviolet band is present in the spectrum of core–shell d:TiO_2–ZnO hierarchical nanofibers, where the presence of monocrystalline ZnO nanoneedles has been unambiguously confirmed by TEM

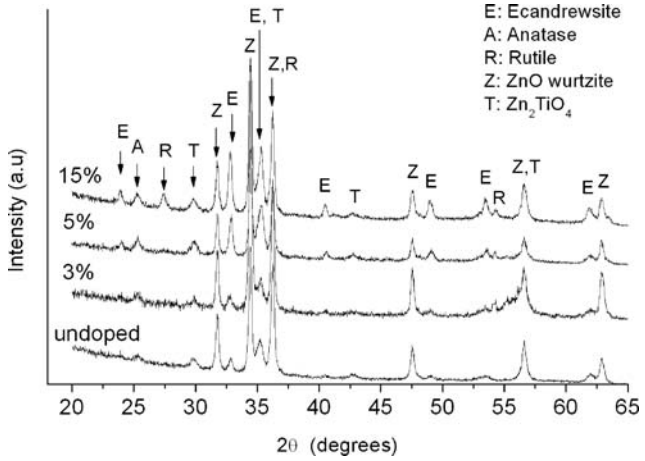

Fig. 7 XRD patterns of the d:TiO_2–ZnO nanofibers.

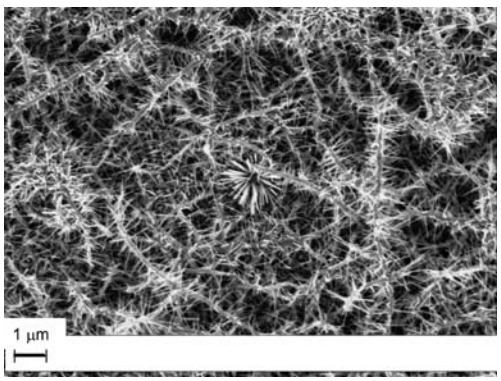

Fig. 8 SEM images of d:TiO_2–ZnO (Zn 3%) nanofibers. The decorating ZnO shell is deposited by MOCVD at 600 °C for 90 min.

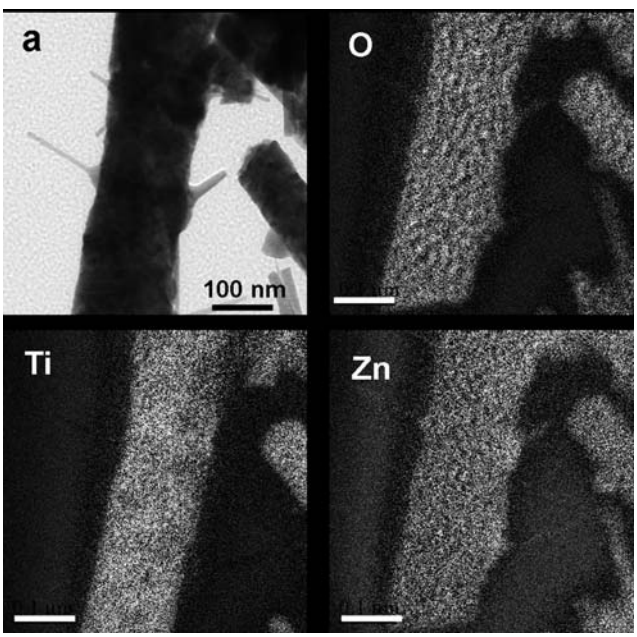

Fig. 9 Bright field TEM image of core–shell d:TiO_2–ZnO (Zn 3%) nanofibers. The decorating ZnO shell is deposited by MOCVD at 600 °C for 90 min (a); Energy Filtered TEM maps for O, Ti and Zn. Scale bar is 100 nm.

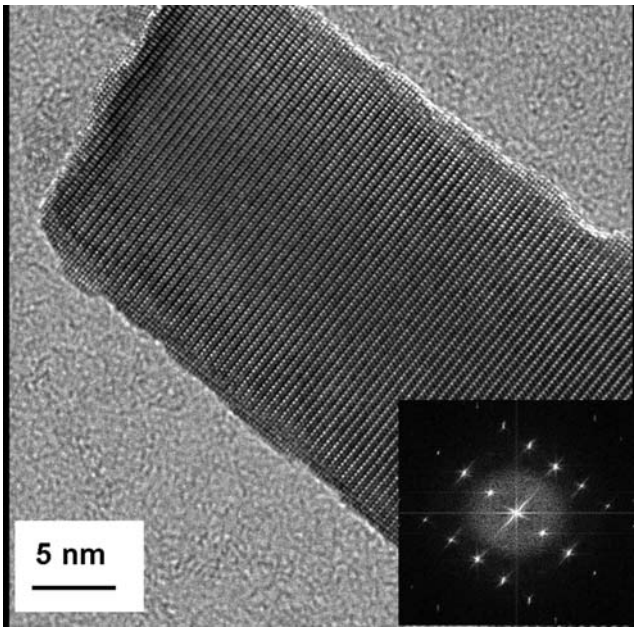

Fig. 10 High Resolution TEM image of core–shell d:TiO_2–ZnO (Zn 3%) nanofibers and the corresponding reduced FFT image (inset).

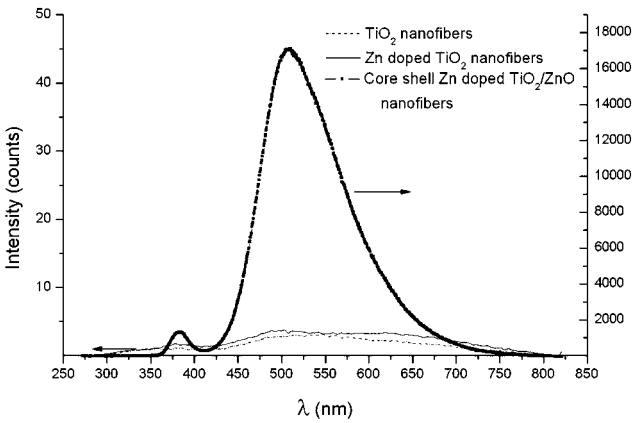

Fig. 11 Cathodoluminescence spectra of TiO_2 and d:TiO_2 (Zn 3%) electrospun nanofibers compared with the spectrum of core–shell d:TiO_2–ZnO (Zn 3%) nanofibers, obtained by depositing the ZnO external shell by MOCVD at 600 °C, 90 min.

analysis (Fig. 10). The intensity of the UV emission[39,44,45] is strongly influenced by the material crystallinity, by the correspondent decrease of impurities and structural defects, as well as by the diameter of emitting nanowires.[46,47] It therefore transpires that the present green emission band intensity observed in the core–shell d:TiO_2–ZnO hierarchical nanofibers, can be correlated to the high surface-to-volume ratio and to the related existence of large quantities of oxygen vacancies within the shelled layers.

Discussions

Recently core–shell nanomaterials have been extensively studied due to their hybrid properties, surface modification and large interfacial area. In particular, TiO_2–ZnO nanocomposites have attracted great attention because the resulting products may

possess improved physical and chemical properties. In this context, the aim of this paper is dual: (i) to find a simple strategy to prepare core–shell TiO_2–ZnO nanofibers; (ii) to identify the issues that affect the nanofiber characteristics in terms of structural and compositional properties. In addition, the effect of Zn doping in the TiO_2 core has been investigated both in regard to the ZnO shell growth and in order to study the transition of anatase to other Ti-containing phases.

One of the most important issues regarding Zn doping is related to the position of Zn within the TiO_2 structure. The Zn^{2+} ion has an ionic radius value (0.74 Å) that is not very different than that of Ti^{4+} (0.68 Å), thus Zn could substitute Ti without producing any important difference in the position of anatase phase peaks in the XRD pattern. This is actually confirmed from XRD patterns, that show the same anatase peak positions for undoped and doped samples, even for the highest concentration (15%). This assumption is also supported by the TEM analysis of the highly doped sample (Zn 15%), which shows a uniform doping distribution inside TiO_2 without evidence of ZnO clusters or aggregates after nanofibers calcination. The slight discernible XPS shift of the Ti 2p core level towards lower binding energy can represent an additional evidence of the Zn doping. The Zn^{2+} ion is also responsible for the higher surface hydroxylation of the doped TiO_2 nanofibers. In this regard it is interesting to note that the Zn/Ti ratio, quantified through XPS, is higher for all the analyzed samples than those expected and confirmed by EDX analyses. This indicates that there is a gradient distribution of Zn^{2+} from the core to the surface. The effect of surface hydroxylation on catalytic activity of semiconductive oxide has been largely discussed,[12] thus pointing to interesting potentiality of the doped nanofibers in this application field. Moreover, it has been observed that Zn doping induces the TiO_2 anatase–rutile transition under the used MOCVD conditions (600 °C, 5 Torr). This finding is in accordance with data previously reported which discuss that aliovalent dopants have an important effect on the formation of defect microstructures and metastable phases in titanium dioxide. [13,14]

Therefore, the ZnO external shell growth will take place on two-phase anatase-rutile composite nanofibers. In fact, XRD patterns indicate that also in the case of core–shell d:TiO_2–ZnO nanofibers the anatase-to-rutile phase transformation occurs under MOCVD processing conditions. The relative anatase/rutile ratio depends upon the Zn content inside the anatase nanofibers.

Apart from this effect, the patterns of core–shell d:TiO_2–ZnO nanofibers present the same peaks although with a different ratio. These findings are found in all the samples independently of the Zn doping. The structural characterization shows in addition to the presence of anatase, rutile and ZnO features, peaks arising from a TiO_2–ZnO phase (ecandrewsite) and Zn_2TiO_4, thus resulting in a nanocomposite architecture.

The amount of Zn-doping slightly affects the morphology. A similar nanostructure with small rounded ZnO grains is observed for the 3 and 5% Zn doping, analogously to the undoped sample. Only for the highest doping level, a different morphology with a nanorod architecture is observed. The morphology is instead affected by the deposition time, having longer time yielding ZnO nanoneedles hierarchical structures. TEM analysis supports the formation of ZnO monocrystalline nanoneedles. These hierarchical nanoarchitectures exhibit a marked CL phenomenon of UV and visible emission.

The obtained results are thus encouraging to propose the present approach as an effective strategy to fabricate multiphase core–shell TiO_2–ZnO nanofibers, which may represent promising materials for photocatalytic applications.

Experimental

Polyvinylpyrrolidone (PVP, Aldrich, MW 1 300 000) solution (7 wt%) was prepared by dissolving PVP powder in ethanol at room temperature under magnetic stirring. The TiO_2 precursor solution was prepared by mixing 1.5 g of titanium tetraisopropoxide ($Ti(OiPr)_4$, Aldrich) with 3 ml of acetic acid and 3 ml of ethanol and stirring for 10 min. The resulting mixture was added to 7.5 ml of PVP solution previously prepared and stirred for a further 10 min. Zn doping was made by mixing the $Ti(OiPr)_4$ and $Zn(tta)_2 \cdot tmeda$ (Htta = 2-thenoyl-trifluoroacetone, tmeda = *N*,*N*,*N*′,*N*′-tetramethylethylendiamine) solutions (3–15% molar). The synthesis of the $Zn(tta)_2 \cdot tmeda$ precursor has been previously reported.[29] The obtained solution was poured in a glass syringe (Hamilton, Carlo Erba) equipped with a 21 G needle, fixed in a digitally controlled syringe pump (KD Scientific, MA, USA). The needle was connected to a high-voltage supply (Spellman, Model SL 30, NY, USA) that is capable of generating DC voltages up to 30 kV. The solution was electrospun in air on a Si substrate and the obtained sample was dried under vacuum for 24 h. The resulting Zn-doped TiO_2/PVP nanofibers (denominated d:TiO_2/PVP) were finally calcined in air at 500 °C for 3 h (heating rate 5 °C min^{-1}, cooling rate 2 °C min^{-1}), in order to completely remove the polymeric component. The obtained Zn-doped TiO_2 (d:TiO_2) ceramic nanofibers were used as template for the following ZnO deposition. A reduced pressure horizontal hot wall MOCVD reactor was used for ZnO decoration of d:TiO_2 nanofibers (d:TiO_2–ZnO). The precursor evaporation temperature and the substrate temperature were maintained at 170 °C and 600 °C, respectively. Ar (250 sccm) and O_2 (250 sccm) were used as carrier and reaction gases, respectively. The mass flows were controlled with a 1160 MKS flowmeter using an MKS147 electronic control unit. Depositions were carried out for 60–90 min. The total pressure in the reactor was about 5 Torr.

θ–2θ X-Ray Diffraction (XRD) patterns were recorded with a Bruker-AXS D5005 θ–θ X-ray diffractometer, using Cu K_α radiation operating at 40 kV and 30 mA.

Morphologies of the undoped TiO_2, d:TiO_2, and d:TiO_2–ZnO nanofibers were investigated using a LEO Supra 55VP field emission scanning electron microscope (FEG-SEM). The atomic composition of the nanofibers was analyzed by energy dispersive X-ray analysis (EDX), using an Oxford solid-state detector. The use of the "windowless" EDX detector is compatible with detection of the O Kα peak at 0.560 KeV.

The elemental chemical distribution was investigated by energy filtered TEM (EF-TEM) analysis by the three windows method using the L edges for the Ti and Zn, and the K edge for O, respectively, employing a TEM JEOL 2010 F instrument.

The X-ray photoelectron experiments (XPS) were carried out with a base pressure of 2×10^{-10} Torr using a PHI ESCA/SAM 5600 Multytechnique spectrometer. A monochromatic Al K_α radiation source ($h\nu$ = 1486.6 eV) was used. The surface analysis

of TiO_2 and d:TiO_2 nanofibers was made in both survey and narrow region scan modes. Zn2p,C1s, Ti2p, O1s and C1s were recorded with 150 eV pass energy, an incremental step size of 1 eV for survey scans and 0.05 eV for the narrow scans, and a 0.8 mm slit width. There was no evidence of charging effects associated with XPS experiments. The XPS signals were analysed with a peak synthesis program assuming a nonlinear background and experimental bounds fitting by a combination of gaussian (80%) and lorentzian (20%) components. The atomic elemental compositions were evaluated using sensitivity factors provided by the F V5.4A software.

Cathodoluminescence (CL) spectra of undoped TiO_2, d:TiO_2 and core–shell d:TiO_2–ZnO nanofibers were excited with a field-emission gun in a conventional scanning electron microscope (FEG-SEM, SE-4300, Hitachi Co. Tokyo, Japan), equipped with a high-sensitivity CL detector unit (MP-32FE, Horiba Ltd. Kyoto, Japan). The CL experiments were performed at 20 kV and 200 pA of probe current. The emitted CL spectrum was analyzed using a monochromator equipped with a CCD camera. A new mapping device (PMT R943-02 Select, Horiba Ltd. Kyoto, Japan) was used and related software was developed to enable collection with nanometre-scale spatial resolution and to automatically analyze a large numbers of CL spectra in near real time.

Conclusions

Zn-doped TiO_2 (d:TiO_2) electrospun nanofibers have been used as template platforms to grow, *via* a MOCVD route, hierarchical ZnO nanoneedles/nanorods. Integration between electrospinning and MOCVD has proven a successful new approach to fabricate heterostructures of highly crystalline ZnO nanostructures and d:TiO_2 anatase/rutile nanofibers. It benefits from all of the advantages of a robust, well reproducible and easily scalable deposition process. Moreover, the appropriate choice of MOCVD operating conditions allows tailoring of the crystalline and morphological structure of the composite nanofibers, thus promoting the anatase-to-rutile TiO_2 transition and/or controlling the morphology of the external shells.

The nanostructured d:TiO_2–ZnO nanofibers have an hydroxyl rich surface and show intense emissions in the UV-Vis regions, thus representing a potentially appealing system for a wide variety of technological fields such as photocatalysts, sensing and optical devices. Work is in progress to extend the electrospinning–MOCVD process integration in the perspective of a suited control of process parameters *vs.* sensing abilities of these d:TiO_2–ZnO core–shell nanofibers.

Acknowledgements

Authors Maria Elena Fragalà and Graziella Malandrino acknowledge the Ministero dello Sviluppo Economico (MSE, Italy) for support of the present study under the ALADIN "Industria 2015" Project.

References

1 Z. L. Wang, *Mater. Sci. Eng.*, 2009, **R64**, 33–71.
2 Z. Z. Ye, F. Yang, Y. F. Lu, M. J. Zhi, H. P. Tang and L. P. Zhu, *Solid State Commun.*, 2007, **142**, 425–428.
3 F. Xu, M. Dai, Y. Lu and L. Sun, *J. Phys. Chem. C*, 2010, **114**, 2776–2782.
4 T. Oekermann, T. Yoshida, C. Boeckler, J. Caro and H. Minoura, *J. Phys. Chem. B*, 2005, **109**, 12560–12566.
5 J. Jinmyoung, L. Dongkyu, Y. Myungsun and J. Sangmin, *Sens. Actuators, B*, 2009, **138**, 485–490.
6 J. Liu, Z. Guo, F. Meng, Y. Jia, T. Luo, M. Li and J. Liu, *Cryst. Growth Des.*, 2009, **9**, 1716–1722.
7 Z. L. Wang, *ACS Nano*, 2008, **2**, 1987–1992.
8 L. S. Wang, M. W. Xiao, X. J. Huang and Y. D. Wu, *J. Hazard. Mater.*, 2009, **161**, 49–54.
9 N. Wang, X. Li, Y. Wang, Y. Hou, X. Zou and G. Chen, *Mater. Lett.*, 2008, **62**, 3691–3693.
10 P. Charoensirithavorn, Y. Ogomi, T. Sagawa, S. Hayase and S. Yoshikawa, *J. Cryst. Growth*, 2009, **311**, 757–759.
11 S. H. Kang, J.-Y. Kim, Y. Kim, H. S. Kim and Y.-E. Sung, *J. Phys. Chem. C*, 2007, **111**, 9614–9623.
12 H. Wang, Z. Wu, Y. Liu and Z. Sheng, *J. Mol. Catal. A: Chem.*, 2008, **287**, 176–181.
13 G. B. Song, J. K. Liang, F. S. Liu, T. J. Peng and G. H. Rao, *Thin Solid Films*, 2005, **491**, 110–116.
14 L. G. Devi, N. Kottam and S. G. Kumar, *J. Phys. Chem. C*, 2009, **113**, 15593–15601.
15 G. Li and K. A. Gray, *Chem. Mater.*, 2007, **19**, 1143–1146.
16 T. Miyagi, M. Kamei, T. Mitsuhashi, T. Ishigaki and A. Yamazaki, *Chem. Phys. Lett.*, 2004, **390**, 399–402.
17 M. C. Carotta, A. Cervi, V. di Natale, S. Gherardi, A. Giberti, V. Guidi, D. Puzzovio, B. Vendemiati, G. Martinelli, M. Sacerdoti, D. Calestani, A. Zappettini, M. Zha and L. Zanotti, *Sens. Actuators, B*, 2009, **137**, 164–169.
18 Y. Zhang, J. Xu, Q. Xiang, H. Li, Q. Pan and P. Xu, *J. Phys. Chem. C*, 2009, **113**, 3430–3435.
19 E. Oh, H-Y. Choi, S-H. Jung, S Cho, J. C. Kim, K-H. Lee, S-W. Kang, J Kim, J.-Y. Yun and S.-H. Jeong, *Sens. Actuators, B*, 2009, **141**, 239–243.
20 Y. Feng, S. Wang, B. Feng, R. Wang, Y. He and T. Zhang, *Sens. Actuators, A*, 2009, **152**, 104–109.
21 F. Fang, J. Futter, A. Markwitz and J. Kennedy, *Nanotechnology*, 2009, **20**, 245502–245508.
22 S. Chuangchote, T. Sagawa and S. Yoshikawa, *Appl. Phys. Lett.*, 2008, **93**, 033310.
23 J. Y. Park, S-W. Choi, J-W. Lee, C. Lee and S. S. Kim, *J. Am. Ceram. Soc.*, 2009, **92**, 2551–2554.
24 W. Wang, H. Huang, Z. Li, H. Zhang, Y. Wang, W. Zheng and C. Wang, *J. Am. Ceram. Soc.*, 2008, **91**, 3817–3819.
25 E. Formo, E. Lee, D. Campbell and Y. Xia, *Nano Lett.*, 2008, **8**, 668–672.
26 N. Wang, C. Sun, Y. Zhao, S. Zhou, P. Chena and L. Jiang, *J. Mater. Chem.*, 2008, **18**, 3909–3911.
27 X. Hu, S. Zhoua and P. Chen, *Chem. Commun.*, 2008, 3293–3295.
28 W. Sigmund, J. Yuh, H. Park, V. Maneeratana, G. Pyrgiotakis, T. J. Daga and J. C. Nino, *J. Am. Ceram. Soc.*, 2006, **89**, 395–407.
29 G. Malandrino, M. Blandino, L. M. S. Perdicaro, I. L. Fragala, P. Rossi and P. Dapporto, *Inorg. Chem.*, 2005, **44**, 9684.
30 B. Erdem, R. A. Hunsicker, G. W. Simmons, E. D. Sudol, V. L. Dimonie and M. S. El-Aasser, *Langmuir*, 2001, **17**, 2664–2669.
31 C.-T. Wang and J.-C. Lin, *Appl. Surf. Sci.*, 2008, **254**, 4500–4507.
32 J.-C. Dupin, D. Gonbeau, P. Vinatier and A. Levasseur, *Phys. Chem. Chem. Phys.*, 2000, **2**, 1319–1324.
33 K. Kotsis and V. Staemmler, *Phys. Chem. Chem. Phys.*, 2006, **8**, 1490–1498.
34 D. Barreca, E. Comini, A. P. Ferrucci, A. Gasparotto, C. Maccato, C. Maragno, G. Sberveglieri and E. Tondello, *Chem. Mater.*, 2007, **19**, 5642–5649.
35 J. Zhao, C. Jia, H. Duan, H. Li and E. Xie, *J. Alloys Compd.*, 2008, **461**, 447–450.
36 M. Foley, C. Ton-That and M. R. Phillips, *Appl. Phys. Lett.*, 2008, **93**, 243104.
37 R. C. Wang, C. P. Liu and J. L. Huang, *Appl. Phys. Lett.*, 2005, **86**, 251104.
38 W. Lehman, *J. Electrochem. Soc.*, 1968, **115**, 538.
39 K. Vanheusden, W. L. Warren, C. H. Seager, D. R. Tallant, J. A. Voigt and B. E. Gnade, *J. Appl. Phys.*, 1996, **79**, 7983–7990.

40 K. Vanheusden, W. L. Warren, C. H. Seager, D. R. Tallant, J. Caruso, M. J. Hampden-Smith and T. T. Kodas, *Mater. Res. Soc. Symp. Proc.*, 1997, **424**, 433.
41 K. Vanheusden, C. H. Seager, W. L. Warren, D. R. Tallant and J. A. Voigt, *Appl. Phys. Lett.*, 1996, **68**, 403–405.
42 A van Dijken, J. Makkinje and A. Meijerink, *J. Lumin.*, 2001, **92**, 323–328.
43 A van Dijken, E. A. Meulenkamp, D. Vanmaekelbergh and A. Meijerink, *J. Phys. Chem. B*, 2000, **104**, 1715–1723.
44 D. Banerjee, J. Y. Lao, D. Z. Wang, J. Y. Huang, D. Steeves, B. Kimball and Z. F. Ren, *Nanotechnology*, 2004, **15**, 404–409.
45 A. L. Pan, R. B. Liu, S. Q. Wang, Z. Y. Wu, L. Cao, S. S. Xie and B. S. Zou, *J. Cryst. Growth*, 2005, **282**, 125–130.
46 M. H. Huang, Y. Y. Wu, N. T. Feick, E. Weber and P. D. Yang, *Adv. Mater.*, 2001, **13**, 113–116.
47 B. D. Yao, Y. F. Chan and N. Wang, *Appl. Phys. Lett.*, 2002, **81**, 757–759.